

The optical properties of dibenzoterrylene

Z. S. Sadeq,* Rodrigo A. Muniz, and J. E. Sipe

Department of Physics, University of Toronto, Toronto, Ontario M5S 1A7, Canada

(Dated: March 14, 2018)

Dibenzoterrylene (DBT) has garnered interest as a potential single photon source (SPS). To have a better grasp of any possible limitations of using DBT for this application, a better understanding of its optical properties is needed. We use a configuration interaction (CI) strategy to calculate the many body wavefunctions of DBT, and we use these wavefunctions to calculate its optical properties. We calculate the linear absorption spectrum and the spatial distributions of electrons involved in several bright transitions. We also calculate the two-photon absorption spectrum of DBT and show that there are several excited states that are bright due to two-photon absorption. Except at high photon energies, we predict that there are no competing optical processes regarding the use of DBT as a SPS. Our calculations provide details of the optical properties of DBT that are interesting in general, and useful for considering optical applications of DBT.

I. INTRODUCTION

Single photon sources (SPSs) are an important resource for optical based quantum information processing [1–7]. Candidate devices are based on semiconductor quantum dots [8–11], color centers in diamond [12–14], and trapped atoms (or ions) in the gas phase [15–17]. Organic materials at cryogenic temperatures also can act as a source of single photons; typically, the optical coherence lifetimes of the relevant transitions in organic materials are longer by an order of magnitude than those of semiconductor quantum dots [3, 18–20]. Synthesis of organic materials is relatively straightforward [21–23]; they are simple to deposit on optical chips and waveguides [24]. Thus organic materials open up the possibility of using existing integrated chip strategies to carry out a variety of nonlinear optical processes [25].

Dibenzoterrylene (DBT) is an organic material that has garnered a lot of interest as a possible SPS [18–20, 25–34]. A cartoon representation of DBT is shown in Fig. 1. Typically, DBT is deposited in an anthracene (Ac) matrix [25, 35], primarily to guard against oxidation and photobleaching, as these processes limit the photostability of the system. DBT has a purely electronic zero phonon line (ZPL) around 785 nm. At low temperatures, the phonon induced dephasing of the transition dipole of the ground state to the first bright excited state, which is labeled S_1 , vanishes [36]; the spectral line width of this transition is then limited only by the radiative lifetime, and DBT can act as a two level system, similar to a trapped atom [3].

The development of DBT as a SPS requires a detailed understanding of its electronic states. In particular, a disadvan-

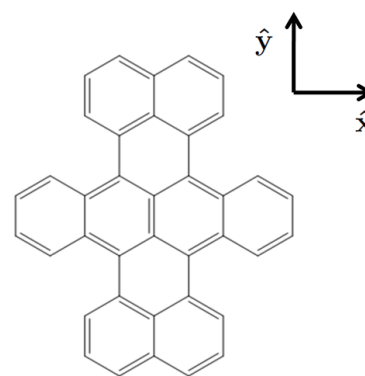


FIG. 1. A cartoon representation of DBT omitting the hydrogen atoms. The two axes, labeled \hat{y} and \hat{x} , are used to facilitate discussions.

tage of using DBT as a SPS is its inter-system crossing (ISC), where the population of a singlet state is funneled to a triplet state [18]. The rate at which ISC proceeds is exponentially suppressed by the energy difference between the singlet state and the triplet state [37–39], and therefore the energy of the triplet state is important in considering the use of DBT as a SPS. There is no consensus on the energy of the first triplet state of DBT, primarily due to experimental limitations. Some researchers have calculated this triplet state to have an energy as low as 0.23 eV above the ground state [40]. This calculated energy is very different from that of the triplet states in the -acenes, materials of similar structure to DBT, which typically have triplet energies on the order of 1 eV above the ground state [41, 42].

There are multiple strategies for calculating the energy of the electronic states of DBT, including Density Matrix Renormalization Group (DMRG) [43–45] and Density Functional

* sadeqz@physics.utoronto.ca

Theory (DFT) [40, 46, 47]. While there have been DMRG studies on the electronic states of systems with similar structure to DBT [43, 44], no calculations have been performed on DBT; with techniques such as DFT, calculations can exhibit large variations in the predicted energies [40, 48]. Crucially, these approaches make it difficult to get a simple picture of the electronic behavior in the excited states. Earlier [49], we used the Pariser-Parr-Pople (PPP) model [50–53] to describe the electronic and optical properties of graphene flakes of similar size and structure to DBT. The PPP model has been successfully implemented to study a range of carbon based materials, from pentacene [43] to graphene flakes [49, 54]. In this paper, we use this same model to elucidate the electronic excited states of DBT. The attractive feature of our approach is its ability to provide a simple physical picture of the electron behavior in these states. We calculate the linear and nonlinear optical absorption of DBT and the electron densities involved in several bright transitions. We demonstrate that there is no other competing one-photon absorption process near the S_1 absorption, and that there are no optical processes that might hinder the application of DBT as a SPS.

This paper is written in four parts: In Section II we discuss the model used to describe the electronic states of DBT, in Section III we compute the one-photon and two-photon absorption of DBT and the spatial distribution of the electrons involved in several bright transitions, and in Section IV we present our conclusions.

II. MODEL AND METHODS

We model the p_z electrons in DBT using the Pariser-Parr-Pople (PPP) Hamiltonian [43, 49–53],

$$H = H_{TB} + H_{Hu} + H_{ext}, \quad (1)$$

where H_{TB} is the tight-binding Hamiltonian, H_{Hu} is the Hubbard Hamiltonian, and H_{ext} is the extended Hubbard Hamiltonian,

$$H_{TB} = - \sum_{\langle i,j \rangle, \sigma} t_{ij} c_{i\sigma}^\dagger c_{j\sigma}, \quad (2)$$

$$H_{Hu} = U \sum_i n_{i\uparrow} n_{i\downarrow}, \quad (3)$$

$$H_{ext} = \frac{1}{2} \sum_{\substack{i \neq j \\ \sigma \sigma'}} V_{ij} \left(n_{i\sigma} - \frac{1}{2} \right) \left(n_{j\sigma'} - \frac{1}{2} \right). \quad (4)$$

Here σ is a spin label, i and j are site labels, and the angular brackets indicate sums over nearest neighbors only. The hopping parameter is set to $t_{ij} = 2.66$ eV for the π conjugated bonds, and $t_{ij} = 2.22$ eV for the single bonds [44, 55]. The fermion creation and annihilation operators are denoted respectively by $c_{i\sigma}^\dagger$ and $c_{i\sigma}$, so the electron number operator for spin σ and site i is $n_{i\sigma} = c_{i\sigma}^\dagger c_{i\sigma}$. The Hubbard repulsion parameter is set to $U = 5.88$ eV for all calculations; this choice of U ensures that the first singlet transition energy matches the experimental value. The value of U we use is similar to values that have been used to model the p_z electrons in other organic systems [49, 50, 54]. We approximate the long-range Coulomb repulsion by the Ohno interpolation [50],

$$V_{ij} = \frac{U}{\sqrt{1 + (4\pi\epsilon_0 U \epsilon r_{ij} / e^2)^2}}, \quad (5)$$

where U is the on-site repulsion parameter, ϵ is a screening parameter, r_{ij} is the distance between sites i and j , $e = -|e|$ is the electronic charge, and ϵ_0 is the vacuum permittivity. We set $\epsilon = 5$ for all calculations, as this value has been used to study similar systems such as graphene flakes [49, 54].

We first consider the Hartree-Fock (HF) approximation for the PPP Hamiltonian (1),

$$\begin{aligned} H^{HF} = & - \sum_{\langle i,j \rangle, \sigma} t_{ij} c_{i\sigma}^\dagger c_{j\sigma} + U \sum_i \left(\langle n_{i\uparrow} \rangle n_{i\downarrow} + \langle n_{i\downarrow} \rangle n_{i\uparrow} - \langle n_{i\uparrow} \rangle \langle n_{i\downarrow} \rangle - \langle c_{i\uparrow}^\dagger c_{i\downarrow} \rangle \langle c_{i\downarrow}^\dagger c_{i\uparrow} \rangle - \langle c_{i\downarrow}^\dagger c_{i\uparrow} \rangle \langle c_{i\uparrow}^\dagger c_{i\downarrow} \rangle + \langle c_{i\uparrow}^\dagger c_{i\downarrow} \rangle \langle c_{i\downarrow}^\dagger c_{i\uparrow} \rangle \right) \\ & + \sum_{i \neq j} V_{ij} \left(n_i \langle n_j \rangle - n_i - \frac{1}{2} \langle n_i \rangle \langle n_j \rangle + \frac{1}{2} - \frac{1}{2} \sum_{\sigma \sigma'} \langle c_{i\sigma}^\dagger c_{j\sigma'} \rangle \langle c_{j\sigma'}^\dagger c_{i\sigma} \rangle + \langle c_{j\sigma'}^\dagger c_{i\sigma} \rangle \langle c_{i\sigma}^\dagger c_{j\sigma'} \rangle - \langle c_{i\sigma}^\dagger c_{j\sigma'} \rangle \langle c_{j\sigma'}^\dagger c_{i\sigma} \rangle \right), \end{aligned} \quad (6)$$

The derivation of these equations is well known [54, 56–58]. We diagonalize H^{HF} and solve for the expectation values self consistently, using the tight-binding (2) eigenstates as an initial guess. The HF Hamiltonian (6) can then be written in

diagonal form as

$$H^{HF} = \sum_{m\sigma} \hbar\omega_{m\sigma} C_{m\sigma}^\dagger C_{m\sigma}, \quad (7)$$

where $\hbar\omega_{m\sigma}$ are the eigenvalues associated with the single par-

particle states, and $C_{m\sigma}^\dagger$ is the corresponding creation operator for a particle with spin σ . The operators $C_{m\sigma}^\dagger$ and $C_{m\sigma}$ can be written in terms of the site basis operators as

$$C_{m\sigma}^\dagger = \sum_i M_{m\sigma,i} c_{i\sigma}^\dagger, \quad (8)$$

$$C_{m\sigma} = \sum_i M_{m\sigma,i}^* c_{i\sigma}, \quad (9)$$

where $M_{m\sigma,i}$ is the amplitude associated with the state m at site i , and is typically non-zero for all i . Since M_σ is a unitary matrix, the HF quasiparticle operators obey the fermionic anticommutation relations $\{C_{m\sigma}, C_{m'\sigma'}^\dagger\} = \delta_{mm'}\delta_{\sigma\sigma'}$. The single particle states obtained from solving the HF equations with paramagnetic expectation values are then used to construct the HF ground state. Single-particle states that are filled in the HF ground state are denoted as “valence”, and the unfilled ones are denoted as “conduction”. We then rewrite the total Hamiltonian (1) in an electron-hole basis. In the electron-hole basis, the HF electron creation operator is designated by $a_{m\sigma}^\dagger$, and the HF hole creation operator is designated by $b_{m'\sigma'}^\dagger$, so

$$a_{m\sigma} = C_{m\sigma}, \quad b_{m'\sigma'}^\dagger = C_{m'\sigma'}, \quad (10)$$

where $\tilde{\sigma}$ is the opposite spin of σ , m indicates a conduction state, and m' indicates a valence state.

To solve for the many body wavefunctions of the system, we restrict the many body Hamiltonian (1) to a set of states following the configuration interaction (CI) method: We employ a basis consisting of the HF ground state, and HF single and double excitations. Upon diagonalization of the many body Hamiltonian, the CI ground state and the CI excited states are superpositions of the HF ground state and the HF excited states. We then diagonalize the many body Hamiltonian (1) restricted to the selected states to obtain the many body wavefunctions. The details of the electron hole basis, and the CI strategy used to solve for the many body wavefunctions, can be found in our earlier work [49]. For the rest of this paper, we shall refer to the HF single particle states as “modes”, and we shall refer to states that result from the CI calculation simply as “states”.

States and Transitions of Interest

We label the first four bright excited states in ascending energy as the S_n states, where $n = \{1, 2, 3, 4\}$. For the application of DBT as a SPS, the transition from the ground state to the S_1 state, denoted $GS \rightarrow S_1$, is the transition of interest; the relaxation of the excitation from the S_1 state to the GS is the source of single photons [25]. We label the lowest energy

two-photon active state as the $2LH$ state; this state is primarily composed of a HF double excitation that excites two electrons from the highest occupied HF mode to the lowest unoccupied HF mode. The next two two-photon active states in order of increasing energy are labeled as S_{D_1} and S_{D_2} ; these states are composed mainly of HF single excitations. We denote the first triplet state as T_1 . The electronic population in the S_1 state can decay to the T_1 state via ISC [39]; the energy of the T_1 state is important as it represents a source of loss for the SPS application. The energies of these states above the ground state are shown in the plot in Fig. 2 (b).

Optical Response

The number operator for a particular site i is

$$n_i = \sum_\sigma c_{i\sigma}^\dagger c_{i\sigma}, \quad (11)$$

and in the electron-hole basis [49], it is written as

$$n_i = \sum_{mm'\sigma} \Gamma_{mm'\sigma,i} (a_{m\sigma}^\dagger a_{m'\sigma} - b_{m'\sigma}^\dagger b_{m\sigma}) + \sum_{mm'\sigma} \Gamma_{mm'\sigma,i} (a_{m\sigma}^\dagger b_{m'\tilde{\sigma}}^\dagger + b_{m\tilde{\sigma}} a_{m'\sigma}) + \sum_{m\sigma} \Gamma_{mm\sigma,i}, \quad (12)$$

where we have defined

$$\Gamma_{mm'\sigma,i} = M_{m\sigma,i} M_{m'\sigma,i}^*. \quad (13)$$

The dipole moment operator of the system is approximated as

$$\boldsymbol{\mu} = \sum_i e \mathbf{r}_i (n_i - 1), \quad (14)$$

where \mathbf{r}_i is the location of site i . Transforming into the electron-hole basis [49], we have

$$\begin{aligned} \boldsymbol{\mu} = & \sum_{m\sigma} \boldsymbol{\mu}_{mm\sigma} - e \sum_i \mathbf{r}_i + \sum_{mm'\sigma} \boldsymbol{\mu}_{mm'\sigma} a_{m\sigma}^\dagger a_{m'\sigma} \\ & - \sum_{mm'\sigma} \boldsymbol{\mu}_{mm'\sigma} b_{m'\sigma}^\dagger b_{m\sigma} + \sum_{mm'\sigma} \boldsymbol{\mu}_{mm'\sigma} a_{m\sigma}^\dagger b_{m'\tilde{\sigma}}^\dagger \\ & + \sum_{mm'\sigma} \boldsymbol{\mu}_{mm'\sigma} b_{m\tilde{\sigma}} a_{m'\sigma}, \end{aligned} \quad (15)$$

where

$$\boldsymbol{\mu}_{mm'\sigma} = \sum_i e \mathbf{r}_i \Gamma_{mm'\sigma,i}. \quad (16)$$

The matrix elements of the dipole moment operator arise in calculating the optical absorption of the material, to which we now turn.

Linear Response

The one-photon absorption spectrum can be determined from the imaginary component of the first order polarizability of the system [59]; assuming the system is initially in the ground state, the imaginary component of the first order polarizability [60] is given by

$$\text{Im}(\alpha_{kl}^{(1)}(\omega)) = \frac{1}{\epsilon_0 \hbar} \sum_m \frac{\gamma_{mg} \mu_{gm}^k \mu_{mg}^l}{(\omega_{mg} - \omega)^2 + \gamma_{mg}^2}, \quad (17)$$

where ω is the frequency, k, l are Cartesian components, ϵ_0 is the vacuum permittivity, μ_{mg} is the matrix element of the dipole moment operator between the ground state and the state m , ω_{mg} is the frequency difference between the state m and the ground state, and γ_{mg} is the frequency broadening associated with the transition from the ground state to the state m . The one-photon absorption coefficient measured in experiments is proportional to the imaginary component of the linear susceptibility of the system [61], which can be obtained from the linear polarizability [59]. We report the predicted strength of each one-photon absorption peak in terms of the oscillator strength associated with the corresponding transition. The predicted oscillator strength of the absorption peak due to the transition from the ground state to the state Y [62], denoted by $GS \rightarrow Y$, is

$$f_{Yg} = \frac{2m_e \omega_{Yg} |\mu_{Yg}|^2}{3\hbar e^2}, \quad (18)$$

where m_e is the electron mass.

We define the “spatial profile” of the transition $GS \rightarrow Y$ as a function $\mathcal{T}_{Y;i}$ of site i given by

$$\mathcal{T}_{Y;i} = \langle Y | n_i | GS \rangle, \quad (19)$$

where GS is the ground state, i is the site, and Y is an excited state. This quantity is related to the matrix element of the dipole moment operator between the ground state and the state Y , the “transition dipole moment”,

$$\langle Y | \mu | GS \rangle = \sum_i e \mathbf{r}_i \mathcal{T}_{Y;i}, \quad (20)$$

where the sum is over all sites i .

Nonlinear Response

The two-photon absorption spectrum can be determined from the imaginary component of the third order polarizability of the system [59]; assuming the system is initially in the ground state, the largest contribution to the third order polarizability for two-photon absorption [63] is given by

$$\alpha_{klop}^{(3)}(\omega; \omega, \omega, -\omega) \approx \frac{1}{\epsilon_0 \hbar^3} \mathcal{P}_I \sum_{vnm} \frac{\mu_{gv}^k \mu_{vn}^l \mu_{nm}^o \mu_{mg}^p}{(\omega_{vg} - \omega - i\gamma_{vg})(\omega_{ng} - 2\omega - i\gamma_{ng})(\omega_{mg} - \omega - i\gamma_{mg})}, \quad (21)$$

where \mathcal{P}_I is the permutation operator in the set of distinct frequencies $\{\omega, \omega, -\omega\}$, $\hbar\omega_{vm}$ is the energy difference between states v and m , and γ_{vg} is the frequency broadening associated with the transition $GS \rightarrow v$. The two-photon absorption coefficient measured in experiments is proportional to the imaginary component of the third order susceptibility of the system [61], which can be obtained from the third order polarizability [59]. The predicted strength of the two-photon transition from the ground state to the state Z is given by

$$B_{klop}(GS \rightarrow Z) = \frac{\pi}{2\epsilon_0 \hbar^3} \sum_{vm} \frac{\mu_{gv}^k \mu_{vZ}^l \mu_{Zm}^o \mu_{mg}^p}{(\omega_{vg} - \bar{\omega})(\omega_{mg} - \bar{\omega})}, \quad (22)$$

where $\bar{\omega} = \omega_{Zg}/2$. A derivation of $B_{klop}(GS \rightarrow Z)$ is presented in Appendix A.

III. OPTICAL ABSORPTION OF DBT

A. Linear Absorption Spectrum and Spatial Profiles of Bright Transitions

In Fig. 2 (a), we plot the oscillator strengths of the bright transitions of DBT assuming the system is initially in the ground state. Recall that the strength of the Coulomb repulsion parameter U was set so the energy of $GS \rightarrow S_1$ is 1.58 eV, in agreement with the experimental value. The radiative line width of $GS \rightarrow S_1$ in vacuum [64] is given by

$$\Gamma_{S_1}^{\text{vac}} = \frac{\omega_{S_1g}^3 |\mu_{S_1g}|^2}{3\pi\epsilon_0 \hbar c^3}, \quad (23)$$

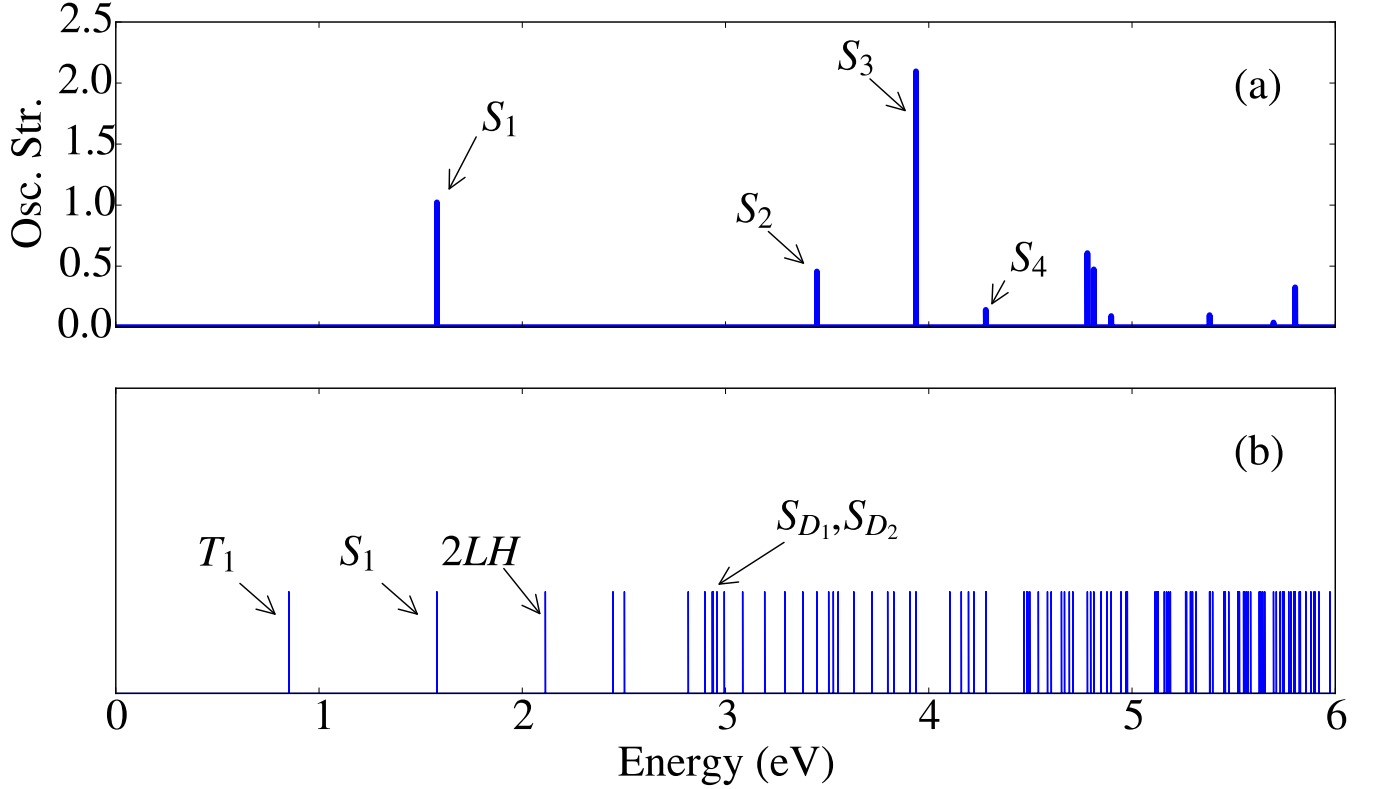


FIG. 2. (a) A plot of the oscillator strengths of the bright transitions, and (b) the energies of the excited states above the ground state of DBT. The parameters of our calculation are set such that the S_1 state is 1.58 eV above the ground state in energy. Our calculation predicts that the T_1 state is 0.85 eV above the ground state in energy. The plot of the energies of the excited states above the ground state indicates that there are no other states below the S_1 state in energy besides the T_1 state. The first absorption peak, due to $GS \rightarrow S_1$, has an associated transition dipole moment which is polarized along the \hat{y} axis. There are several other high energy absorption peaks, the strongest of which is due to $GS \rightarrow S_3$; this transition has a transition dipole moment which is polarized along the \hat{x} axis. However, these bright states are all more than 3 eV above the ground state in energy, which is around twice the energy of the $GS \rightarrow S_1$ transition. The axes are shown in Fig. 1.

where c is the speed of light, $\omega_{S_{1g}}$ is the frequency difference between the S_1 state and the ground state, and $|\mu_{S_{1g}}|$ is the magnitude of the matrix element of the dipole moment operator between the ground state and the S_1 state; we find $|\mu_{S_{1g}}| = 13.1$ Debye. Due to local field effects, the radiative line width of $GS \rightarrow S_1$ is modified when DBT is deposited in an anthracene matrix. There is some controversy as to which is the most appropriate model to describe the local field effects when calculating the radiative line width of emitters embedded in a homogeneous medium [65, 66]. The real cavity model describes local field effects when the emitters, in this case the DBT molecules, enter the medium as dopants [65, 66]. Accounting for local field effects using the real cavity model, the radiative line width of the $GS \rightarrow S_1$ transition is

$$\Gamma_{S_1}^{\text{RC}} = n_{\text{eff}} \left(\frac{3n_{\text{eff}}^2}{2n_{\text{eff}}^2 + 1} \right)^2 \Gamma_{S_1}^{\text{vac}}, \quad (24)$$

where n_{eff} is the effective refractive index of the material. Since the concentration of DBT in the anthracene matrix is extremely dilute [23, 25], we take n_{eff} to be the refractive index of anthracene. Using Eq. (24), we calculate the radiative line width of $GS \rightarrow S_1$ to be 40 MHz; a complete neglect of local field corrections leads to a predicted radiative line width of 30 MHz. Measurements of the homogeneously broadened radiative line width of the $GS \rightarrow S_1$ transition range from 30-40 MHz [3, 19, 34]. These measurements were carried out at cryogenic temperatures, at which the radiative line width is generally assumed to be limited only by the excited state lifetime [3, 67]. Given that our calculated radiative line width is in the range of reported experimental values, and assuming the experimental value of the radiative line width is indeed limited only by the excited state lifetime, then the magnitude of our calculated $GS \rightarrow S_1$ transition dipole moment is also consistent with the experimental values.

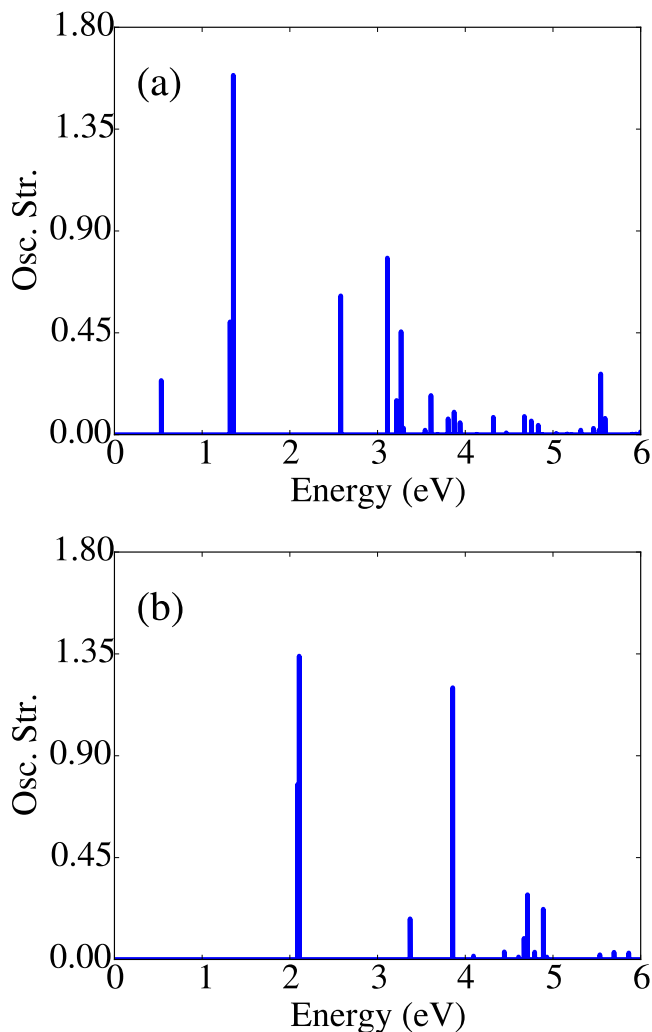


FIG. 3. The oscillator strengths of the bright transitions with (a) the first singlet state S_1 , and (b) the first triplet state T_1 , as the initial state. Further absorption from the S_1 or T_1 state does not fall within the energy range of the transition from the ground state to the S_1 state.

In our calculations, the lowest triplet state, T_1 , has energy 0.85 eV above the ground state, which is about half the energy of the first singlet excited state above the ground state. The energy of the triplet state is calculated to be greater than the corresponding value calculated by Deperasinska *et al.* [40] by 0.62 eV. Their calculation predicts that the T_1 state is 0.23 eV above the ground state; however, they point out that the method they use to calculate the energies of the excited states exhibits an average deviation of 0.4 eV between the calculated energies and the experimental values for small molecules, and gives less accurate results for systems as large as DBT [40, 46, 47]. The energies of the lowest triplet excited states in the -acene series, which are similar in structure

to DBT, are approximately 1 eV above the ground state [42]; in the -acene series, the energy above the ground state of the lowest triplet excited state is approximately half of the energy above the ground state of the lowest singlet excited state, as we find for DBT. The energy of the triplet state in DBT has yet to be experimentally determined. Absorption to the other excited states requires photon energies greater than 3 eV. Our calculations indicate that there are no other absorption peaks close in energy to the absorption peak due to $GS \rightarrow S_1$, and we predict that there are no competing linear optical processes that might reduce the efficacy of the application of this material as a SPS. The plot of the energies of the excited states above the ground state, shown in Fig. 2 (b), indicates that there are no other excited states that are lower in energy than the S_1 state, except for the T_1 state. Thus from our calculations the only other major relaxation channel is the ISC to the T_1 state.

To consider the possible significance of sequential absorption from the ground state, we investigate the oscillator strengths of the bright transitions with (a) S_1 and (b) T_1 as the initial state. We plot these oscillator strengths in Fig. 3. It is clear that further absorption from the S_1 state either occurs at photon energies below (less than 0.5 eV) or above (greater than 2 eV) the energy of $GS \rightarrow S_1$. If the excitation decays to the triplet state, due to ISC for example, any further absorption from the triplet state occurs at photon energies that are much higher (greater than 2 eV) than the energy of $GS \rightarrow S_1$. Our calculations indicate that there is no further absorption from the S_1 or T_1 state for the energy range of interest of the application of DBT as a SPS.

Finally, we turn to the spatial profiles of the bright transitions from the ground state of DBT. We calculate $\mathcal{T}_{Y;i}$ for the first four bright excited states, and plot them in Fig. 4. The molecular axes are shown in Fig. 1. The transition dipole moments associated with the first two optical transitions, $GS \rightarrow S_1$ and $GS \rightarrow S_2$, are polarized along the \hat{y} axis. The spatial profile of $GS \rightarrow S_1$ has electron density extended across the entire system and leads to a very large transition dipole moment. The spatial profile of $GS \rightarrow S_2$ has electron concentration extended across the entire system, much like $\mathcal{T}_{S_1;i}$, but has a weaker transition dipole moment. The transition dipole moments associated with the next two optical transitions, $GS \rightarrow S_3$ and $GS \rightarrow S_4$, are polarized along the \hat{x} axis. The spatial profile of $GS \rightarrow S_3$ has electron density primarily on the four rings in the middle of the system, and it has very little concentration on the top and bottom rings; it leads to a very large transition dipole moment. The spatial profile of $GS \rightarrow S_4$ has significant electron concentration in

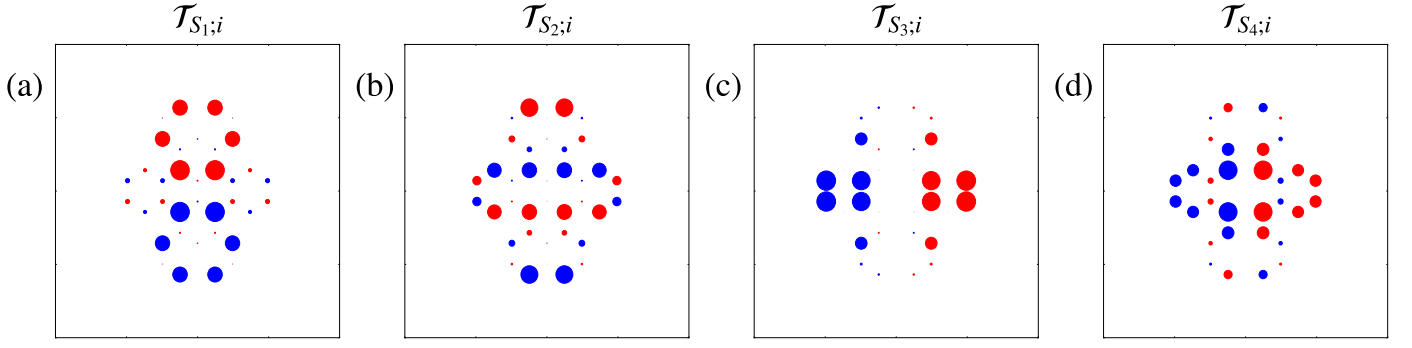


FIG. 4. Plots of (a) $\mathcal{T}_{S_1;i}$, (b) $\mathcal{T}_{S_2;i}$, (c) $\mathcal{T}_{S_3;i}$, and (d) $\mathcal{T}_{S_4;i}$. We place a circle at the location of each site i ; the area of each circle indicates the magnitude of $\mathcal{T}_{S_i;i}$, and the color indicates whether it is positive (red) or negative (blue). The convention used for labeling these states follows energetic order, i.e. S_1 is the lowest energy state, S_2 is the second lowest energy state and so on. The transitions that are polarized along the \hat{y} axis have electron concentration extended throughout the system, while those polarized along the \hat{x} axis have electron concentration primarily in the middle of the system; the axes are shown in Fig. 1.

the middle of the system, and it has negligible electron concentration in the top and bottom rings of the system; it leads to a weaker transition dipole moment. For transitions with dipole moment polarized along the \hat{y} axis, the electron density is extended across the entire system, but for transitions with dipole moment polarized along the \hat{x} axis, the electron density is concentrated at the center of the system.

B. Two-Photon Absorption Spectrum

Transition	$\hbar\omega$ (eV)	Strength ($\mu\text{m}^5/\text{V}^2\text{s}$)	Component
$GS \rightarrow 2LH$	1.06	0.599	yyyy
$GS \rightarrow S_{D_1}$	1.45	8.08	yxxxy
$GS \rightarrow S_{D_2}$	1.47	33.8	yyyy

TABLE I. The lowest three two-photon transitions of DBT, their associated fundamental photon energies $\hbar\omega$, the associated integrated third order polarizability strengths, and the component of the third order polarizability tensor that exhibit the peaks.

For the two-photon transitions of interest, we compute their associated fundamental photon energies, two-photon transition strengths, and the components of the third order polarizability tensor that exhibit the peaks. In Table I we show the values of these quantities. The lowest energy TPA is due to $GS \rightarrow 2LH$, and arises from $\text{Im}(\alpha_{yyyy}^{(3)})$; the $2LH$ state is composed mainly of HF double excitations. The next two TPA peaks are due to $GS \rightarrow S_{D_1}$ (from $\text{Im}(\alpha_{yxxxy}^{(3)})$) and $GS \rightarrow S_{D_2}$ (from $\text{Im}(\alpha_{yyyy}^{(3)})$); the S_{D_1} state and the S_{D_2} state are composed mainly of HF single excitations. The two-photon transitions $GS \rightarrow S_{D_1}$ and $GS \rightarrow S_{D_2}$ occur when the fundamental pho-

ton energy $\hbar\omega$ is close to the energy of the single photon transition $GS \rightarrow S_1$. The calculated strength of the TPA in DBT is in line with the TPA calculated in other conjugated organic systems [42, 68].

From the values of the calculated energies and the calculated absorption strengths, we argue that for the SPS application of DBT, the TPA should not compete with $GS \rightarrow S_1$ in any meaningful way.

First we consider that a continuous wave (CW) laser is used to pump $GS \rightarrow S_1$ [25]. Since the spectral width of CW lasers is usually less than 0.01 meV, the spectrum of a CW laser centered at $\omega_{S_{1g}}$ will not contain the frequency components required to excite either S_{D_1} or S_{D_2} .

Second we consider the excitation by optical pulses, as done in a number of experiments [3, 18, 69]. For example, Toninelli *et al.* [18] used a Ti:Sapphire laser with a spectrum centered near $\omega_{S_{1g}}$ and a pulse duration of 120 fs to excite $GS \rightarrow S_1$. The spectrum of these pulses has the necessary frequency components to excite the two-photon active transitions near $GS \rightarrow S_1$. To investigate the possible consequences of TPA, we use a perturbative treatment [70] to calculate the one-photon absorption to the S_1 state and the two-photon absorption to the S_{D_2} state. This approach is a generalization of Eqs. (17) and (21) respectively for pulsed pumping. We model the laser pulse as an unchirped Gaussian centered at $\omega_{S_{1g}}$ with an intensity full width at half maximum (FWHM) of τ . Upon excitation of DBT, the population ρ_{S_1} of the S_1 state at times after the pulse is

$$\rho_{S_1} = \left(\frac{\pi |\mu_{S_{1g}}|^2}{(4 \ln 2) n_{\text{eff}} \epsilon_0 c \hbar^2} \right) \tau^2 I_0, \quad (25)$$

where I_0 is the peak intensity; I_0 can be written in terms of the

pulse energy as

$$I_0 = \frac{2\sqrt{\ln 2}}{\sqrt{\pi}\tau} \frac{Q_{\text{pulse}}}{A_{\text{pulse}}}, \quad (26)$$

where Q_{pulse} is the pulse energy and A_{pulse} is the area of the laser spot. The population $\rho_{S_{D_2}}$ of the S_{D_2} state at such times

is given by

$$\frac{\rho_{S_{D_2}}}{\rho_{S_1}} = \left(\frac{|\mu_{S_{D_2}S_1}|^2 |\mathcal{F}|^2}{(16 \ln 2) \pi n_{\text{eff}} \epsilon_0 c \hbar^2} \right) \tau^2 I_0. \quad (27)$$

Here $|\mu_{S_{D_2}S_1}|$ is the magnitude of the matrix element of the dipole moment operator between the S_1 state and the S_{D_2} state; from our calculations $|\mu_{S_{D_2}S_1}| = 17.6$ Debye. The term \mathcal{F} is

$$\mathcal{F} = \int_{-\infty}^{\infty} \frac{\exp\left(-\frac{\tau^2}{4 \ln 2} (\omega - \omega_{S_{1g}})^2\right) \exp\left(-\frac{\tau^2}{4 \ln 2} (\omega_{S_{D_2g}} - \omega - \omega_{S_{1g}})^2\right)}{(\omega_{S_{1g}} - \omega - i(\Gamma_{S_1}/2))} d\omega, \quad (28)$$

where $\omega_{S_{D_2g}}$ is the frequency difference between the S_{D_2} state and the ground state, and Γ_{S_1} is the linewidth of $GS \rightarrow S_1$ given by (24). For $\tau = 120$ fs, $|\mathcal{F}|^2 \approx 5.58 \times 10^{-4}$.

In a previous experimental study of DBT [18], pulsed lasers with an average power of 3 W, a repetition rate of 76 MHz, and resulting peak intensities ranging from 500-4000 kW/cm² were used to excite $GS \rightarrow S_1$; for these peak intensities, we predict that the ratio of the populations of the S_{D_2} state and the S_1 state (27) is on the order of 10^{-7} . At a peak intensity of 30 MW/cm² (corresponding to a pulse energy of 0.32 nJ and assuming a circular laser spot with a radius of 50 μm), our perturbative assumption (i.e. the excitation by the laser pulse is weak) breaks down, and the predicted population of the S_1 state is large ($\rho_{S_1} \approx 0.2$). For this peak intensity of the pulse, the ratio between the populations of the S_{D_2} state and the S_1 state (27) is on the order of 10^{-6} . This indicates that even for intensities strong enough to significantly populate the S_1 state, the population of the S_{D_2} state will be minuscule relative to the population of the S_1 state.

IV. CONCLUSION

We applied a method developed for the description of the electronic and optical properties of graphene flakes to study the optical properties of dibenzoterrylene (DBT), a candidate material for single photon source (SPS) applications. We set the Hubbard U parameter of our calculation such that the lowest energy singlet excited state, labeled S_1 , is 1.58 eV above the ground state energy, in agreement with the experimental value. Our calculated radiative line width for the transition from the ground state to the S_1 state (denoted $GS \rightarrow S_1$) agrees with the experimental value as well. Assuming the ex-

perimental measurement of the radiative linewidth is limited only by the excited state lifetime, then our calculated value of the $GS \rightarrow S_1$ transition dipole moment is consistent with its experimental value.

For DBT to be a good SPS, there should be no other optical processes that compete with the transition from the ground state to the first singlet excited state: There should be no other linear absorption peaks near the peak due to $GS \rightarrow S_1$; further absorption from the S_1 state should not occur at photon energies near the energy of $GS \rightarrow S_1$; inter-system crossing (ISC) to the first triplet state, labeled T_1 , should not be significant; and further absorption from the T_1 state also should not occur at photon energies near the energy of $GS \rightarrow S_1$.

We calculated the oscillator strengths of the bright transitions of DBT up to 6.0 eV, which should be useful for testing the model against future experiments; excitations from the sp^2 states, not included in this model, are not expected to be in this energy range. Our calculations predict that there are no other competing linear absorption features near the energy of $GS \rightarrow S_1$. We also calculated the further absorption from the S_1 state; our calculations indicate that there is no further absorption from the S_1 state for the energy range of interest in the application of DBT as a SPS. We characterized the charge distributions involved in the bright transitions of DBT, and we showed that the spatial profiles of transitions which have transition dipole moments that are polarized along the \hat{y} axis have electron concentration extended over the entire system, while the spatial profiles of transitions which have transition dipole moments polarized along the \hat{x} axis have electron concentration primarily in the center of the system.

Our calculations indicate that the T_1 state has energy 0.85 eV above the ground state; in our calculation, the energy above the ground state of the T_1 state is approximately half

the energy above the ground state of the S_1 state. Such a large difference in energy between the S_1 state and the T_1 state indicates that the ISC rate is small in DBT [37, 38]. We calculated the further absorption from the T_1 state; our calculations indicate that there is no further absorption from the T_1 state for the energy range of interest in the application of DBT as a SPS.

We also calculated the two-photon absorption (TPA) of DBT. An understanding of the nonlinear optical properties of DBT is important for general optical applications, and also for the specific application of DBT as a SPS since it reveals whether there are any competing nonlinear optical processes against the optical transition that generates the desired photons. The TPA spectrum showed that in the low photon energy regime, three states are two-photon active: a state composed primarily of HF double excitations, and two states composed

mainly of HF single excitations. The strong two-photon absorption occurs at fundamental photon energies near the energy of $GS \rightarrow S_1$. If narrow frequency laser pulses (with a temporal full width at half maximum greater than 120 fs) and weak peak intensities (on the order of 1000 kW/cm²), or continuous wave lasers are used to excite $GS \rightarrow S_1$, then the strong TPA that occurs at photon energies near the energy of $GS \rightarrow S_1$ should not hinder the SPS application of DBT.

Therefore, our calculations indicate that DBT is a good candidate for a SPS, as there are no other competing absorption features near the energy of the transition from the ground state to the S_1 state. The calculations we have performed have also elucidated qualitative features of the higher energy absorption spectrum of DBT, and we expect that these qualitative features will be of interest for considering the use of DBT for other optical applications besides SPS.

Appendix A: Integrated Third Order Polarizability

In this appendix, we derive an expression for the integrated third polarizability. The largest contribution to the third order polarizability [63] is given by

$$\alpha_{klop}^{(3)}(\omega; \omega, \omega, -\omega) \approx \frac{1}{\epsilon_0 \hbar^3} \sum_{vnm} \frac{\mu_{gv}^k \mu_{vn}^l \mu_{nm}^o \mu_{mg}^p}{(\omega_{vg} - \omega - i\gamma_{vg})(\omega_{ng} - 2\omega - i\gamma_{ng})(\omega_{mg} - \omega - i\gamma_{mg})} \quad (A1)$$

near the $\omega_{ng} \approx 2\omega$ resonance. At such frequencies, the third order polarizability (A1) can be further approximated as

$$\alpha_{klop}^{(3)} \approx \frac{1}{\epsilon_0 \hbar^3} \sum_{vnm} \frac{\mu_{gv}^k \mu_{vn}^l \mu_{nm}^o \mu_{mg}^p}{(\omega_{vg} - \bar{\omega})(\omega_{mg} - \bar{\omega})} \frac{1}{(\omega_{ng} - 2\omega - i\gamma_{ng})}, \quad (A2)$$

where $\bar{\omega} = \omega_{ng}/2$. The imaginary component of (A2) is given by

$$\text{Im}(\alpha_{klop}^{(3)}) \approx \frac{1}{\epsilon_0 \hbar^3} \sum_{vnm} \frac{\mu_{gv}^k \mu_{vn}^l \mu_{nm}^o \mu_{mg}^p}{(\omega_{vg} - \bar{\omega})(\omega_{mg} - \bar{\omega})} \frac{\gamma_{ng}}{(\omega_{ng} - 2\omega)^2 + \gamma_{ng}^2}. \quad (A3)$$

Integrating (A3) over all frequencies ω , we obtain

$$\int_{-\infty}^{\infty} \text{Im}(\alpha_{klop}^{(3)}) d\omega \approx \frac{\pi}{2\epsilon_0 \hbar^3} \sum_{vnm} \frac{\mu_{gv}^k \mu_{vn}^l \mu_{nm}^o \mu_{mg}^p}{(\omega_{vg} - \bar{\omega})(\omega_{mg} - \bar{\omega})}, \quad (A4)$$

where we have used $\int_{-\infty}^{\infty} 1/((2x - x_0)^2 + \gamma^2) dx = \pi/2\gamma$. The expression (A4) is the integrated third order polarizability, which is independent of the frequency broadening γ . Therefore, the strength of the two photon transition $GS \rightarrow Z$ is given by

$$B_{klop}(GS \rightarrow Z) = \frac{\pi}{2\epsilon_0 \hbar^3} \sum_{vm} \frac{\mu_{gv}^k \mu_{vZ}^l \mu_{Zm}^o \mu_{mg}^p}{(\omega_{vg} - \bar{\omega})(\omega_{mg} - \bar{\omega})}, \quad (A5)$$

which is Eq. (22).

-
- [1] M. D. Eisaman, J. Fan, A. Migdall, and S. V. Polyakov, *Review of Scientific Instruments* **82**, 071101 (2011).
- [2] M. Schiavon, G. Vallone, F. Ticozzi, and P. Villoresi, *Phys. Rev. A* **93**, 012331 (2016).
- [3] J.-B. Trebbia, H. Ruf, P. Tamarat, and B. Lounis, *Opt. Exp.* **17**, 23986 (2009).
- [4] B. Lounis and M. Orrit, *Rep. Prog. Phys.* **68**, 1129 (2005).
- [5] J. L. O'Brien, *Science* **318**, 1567 (2007).
- [6] C. Kurtsiefer, S. Mayer, P. Zarda, and H. Weinfurter, *Phys. Rev. Lett.* **85**, 290 (2000).
- [7] I. Aharonovich, A. D. Greentree, and S. Prawer, *Nature Photonics* **5**, 397 (2011).
- [8] M. Müller, H. Vural, C. Schneider, A. Rastelli, O. G. Schmidt, S. Höfling, and P. Michler, *Phys. Rev. Lett.* **118**, 257402 (2017).
- [9] S. Buckley, K. Rivoire, and J. Vučković, *Rep. Prog. Phys.* **75**, 126503 (2012).
- [10] P. Senellart, G. Solomon, and A. White, *Nature Nanotechnology* **12**, 1026 (2017).
- [11] D. C. Unitt, A. J. Bennett, P. Atkinson, K. Cooper, P. See, D. Gevaux, M. B. Ward, R. M. Stevenson, D. A. Ritchie, and A. J. Shields, *J. Opt. B: Quantum Semiclass. Opt.* **7**, S129 (2005).
- [12] C. Wang, C. Kurtsiefer, H. Weinfurter, and B. Burchard, *J. Phys. B: At. Mol. Opt. Phys.* **39**, 37 (2006).
- [13] I. A. Khramtsov, M. Agio, and D. Y. Fedyanin, *Phys. Rev. Applied* **8**, 024031 (2017).
- [14] L. Marseglia, K. Saha, A. Ajoy, T. Schröder, D. Englund, F. Jelezko, R. Walsworth, J. L. Pacheco, D. L. Perry, E. S. Bielejec, and P. Cappellaro, *Opt. Express* **26**, 80 (2018).
- [15] D. B. Higginbottom, L. Slodička, G. Araneda, L. Lachman, R. Filip, M. Hennrich, and R. Blatt, *New J. Phys.* **18**, 093038 (2016).
- [16] M. Hijkema, B. Weber, H. P. Specht, S. C. Webster, A. Kuhn, and G. Rempe, *Nature Physics* **3**, 253 (2007).
- [17] M. Keller, B. Lange, K. Hayasaka, W. Lange, and H. Walther, *Nature* **431**, 1075 (2004).
- [18] C. Toninelli, K. Early, J. Breimi, A. Renn, S. Götzinger, and V. Sandoghdar, *Opt. Exp.* **18**, 6577 (2010).
- [19] A. A. L. Nicolet, P. Bordat, C. Hofmann, M. A. Kol'chenko, B. Kozankiewicz, R. Brown, and M. Orrit, *ChemPhysChem* **8**, 1929 (2007).
- [20] A.-M. Boiron, F. Jelezko, Y. Durand, B. Lounis, and M. Orrit, *Mol. Cryst. Liq. Cryst.* **291**, 41 (1996).
- [21] S. Faez, N. R. Verhart, M. Markoulides, F. Buda, A. Gourdon, and M. Orrit, *Faraday Discussions* **184**, 251 (2015).
- [22] Y. Li, Z. Jia, S. Xiao, H. Liu, and Y. Li, *Nature Communications* **7**, 11637 (2016).
- [23] K. D. Major, Y.-H. Lien, C. Polisseni, S. Grandi, K. W. Kho, A. S. Clark, and E. A. Hinds, *Review of Scientific Instruments* **86**, 083106 (2015).
- [24] P. E. Lombardi, A. P. Ovvyan, S. Pazzagli, G. Mazzamuto, G. Kewes, O. Neitzke, N. Gruhler, O. Benson, W. H. P. Pernice, F. S. Cataliotti, and C. Toninelli, *ACS Photonics* **5**, 126 (2018).
- [25] C. Polisseni, K. D. Major, S. Boissier, S. Grandi, A. S. Clark, and E. A. Hinds, *Opt. Exp.* **24**, 5615 (2016).
- [26] Y. Tian, P. Navarro, B. Kozankiewicz, and M. Orrit, *ChemPhysChem* **13**, 3510 (2012).
- [27] P. Siyushev, G. Stein, J. Wrachtrup, and I. Gerhardt, *Nature* **509**, 66 (2014).
- [28] J. Hwang and E. A. Hinds, *New J. Phys.* **13**, 085009 (2011).
- [29] D. Wang, H. Kelkar, D. Martin-Cano, T. Utikal, S. Götzinger, and V. Sandoghdar, *Phys. Rev. X* **7**, 021014 (2017).
- [30] N. R. Verhart, M. Müller, and M. Orrit, *ChemPhysChem* **17**, 1524 (2016).
- [31] F. Jelezko, P. Tamarat, B. Lounis, and M. Orrit, *J. Phys. Chem.* **100**, 13892 (1996).
- [32] C. Hofmann, A. A. L. Nicolet, M. A. Kol'chenko, and M. Orrit, *Chemical Physics* **318**, 1 (2005).
- [33] A. A. L. Nicolet, M. A. Kol'chenko, C. Hofmann, B. Kozankiewicz, and M. Orrit, *Physical Chemistry Chemical Physics* **15**, 4415 (2013).
- [34] S. Grandi, K. D. Major, C. Polisseni, S. Boissier, A. S. Clark, and E. A. Hinds, *Phys. Rev. A* **94**, 063839 (2016).
- [35] A. Makarewicz, I. Deperasinska, E. Karpiuk, J. Nowacki, and B. Kozankiewicz, *Chem. Phys. Lett.* **535**, 140 (2012).
- [36] B. Kozankiewicz and M. Orrit, *Chem. Phys. Rev.* **43**, 1029 (2014).
- [37] R. Englman and J. Jortner, *Molecular Physics* **18**, 145 (1970).
- [38] C. M. Marian, *WIREs Comput. Mol. Sci.* **2**, 187 (2012).
- [39] J. D. Coyle, *Introduction to Organic Photochemistry* (Wiley, New York, 1989).
- [40] I. Deperasinska, E. Karpiuk, M. Banasiewicz, and B. Kozankiewicz, *Chem. Phys. Lett.* **492**, 93 (2010).
- [41] M. B. Smith and J. Michl, *Ann. Rev. Phys. Chem.* **64**, 361 (2013).
- [42] Z. S. Sadeq and J. E. Sipe, arXiv:1511.09396.
- [43] C. Raghu, Y. A. Pati, and S. Ramasesha, *Phys. Rev. B* **65**, 155204 (2002).
- [44] J. Hachmann, J. Dorando, M. Aviles, and G. K.-L. Chan, *J. Chem. Phys.* **127**, 134309 (2007).
- [45] I. Hagymási and O. Legeza, *Phys. Rev. B* **94**, 165147 (2016).
- [46] J. Fabian, L. A. Diaz, G. Seifert, and T. Niehaus, *J. Mol. Struct. THEOCHEM* **594**, 41 (2002).
- [47] L. Serrano-Andrés and M. Merchán, *J. Mol. Struct. THEOCHEM* **729**, 99 (2005).
- [48] Y. X. Yao, J. Liu, C. Liu, W. C. Lu, C. Z. Wang, and K. M. Ho, *Scientific Reports* **5**, 13478 (2015).
- [49] Z. S. Sadeq, R. A. Muniz, and J. E. Sipe, *Phys. Rev. Materials* **2**, 014001 (2018).

- [50] W. Barford, *Electronic and Optical Properties of Conjugated Polymers*, 1st ed. (Oxford University Press, New York, 2005).
- [51] R. Pariser and R. G. Parr, J. Chem. Phys. **21**, 466 (1953).
- [52] R. Pariser and R. G. Parr, J. Chem. Phys. **21**, 767 (1953).
- [53] J. A. Pople, Proc. Phys. Soc. **68**, 81 (1954).
- [54] J. Vergés, G. Chiappe, and E. Louis, Eur. Phys. J. B. **88**, 200 (2015).
- [55] R. Kundu, Mod. Phys. Lett. B **25**, 163 (2011).
- [56] H. Bruus and K. Flensberg, *Many-body Quantum Theory in Condensed Matter Physics* (Oxford University Press, New York, 2004).
- [57] G. F. Giuliani and G. Vignale, *Quantum Theory of the Electron Liquid* (Cambridge University Press, New York, 2005).
- [58] D. Pines, *Elementary Excitations in Solids* (W.A. Benjamin Inc., New York, 1977).
- [59] R. W. Boyd, *Nonlinear Optics* (Academic Press Inc., San Diego, 2008).
- [60] R. W. Boyd, *Nonlinear Optics* (Academic Press Inc., San Diego, 2008) pp. 164.
- [61] J. Wei, *Nonlinear Super-Resolution Nano-Optics and Applications* (Springer, New York, 2015).
- [62] R. W. Boyd, *Nonlinear Optics* (Academic Press Inc., San Diego, 2008) pp. 166.
- [63] R. W. Boyd, *Nonlinear Optics* (Academic Press Inc., San Diego, 2008) pp. 183.
- [64] R. W. Boyd, *Nonlinear Optics* (Academic Press Inc., San Diego, 2008) pp. 169.
- [65] K. Dolgaleva, R. W. Boyd, and P. W. Milonni, J. Opt. Soc. Am. B **24**, 516 (2007).
- [66] K. Dolgaleva and R. W. Boyd, Advances in Optics and Photonics **4**, 1 (2012).
- [67] T. Basché, S. Kummer, and C. Bräuchle, “Excitation and emission spectroscopy and quantum optical measurements,” (VCH Verlagsgesellschaft mbH, 2007) pp. 31–67.
- [68] K. Aryanpour, A. Roberts, A. Sandhu, R. Rathore, A. Shukla, and S. Mazumdar, J. Phys. Chem. C **118**, 3331 (2014).
- [69] A. S. Clark, S. Boissier, C. Polisseni, S. Grandi, K. Major, and E. A. Hinds, in *Advanced Photonics 2016 (IPR, NOMA, Sensors, Networks, SPPCom, SOF)* (Optical Society of America, 2016) p. IW3B.6.
- [70] D. J. Tannor, *Introduction to Quantum Mechanics: A Time-Dependent Perspective* (University Science Books, Sausalito, 2006).